Directly generating orbital angular momentum in second-harmonic waves with a spirally poled nonlinear photonic crystal

Dunzhao Wei, Yunzhi Zhu, Weihao Zhong, Guoxin Cui, Huijun Wang, Ying He, Yong Zhang, Yanqing Lu, and Min Xiao

Citation: Appl. Phys. Lett. **110**, 261104 (2017); doi: 10.1063/1.4990527
View online: http://dx.doi.org/10.1063/1.4990527
View Table of Contents: http://aip.scitation.org/toc/apl/110/26
Published by the American Institute of Physics

Directly generating orbital angular momentum in second-harmonic waves with a spirally poled nonlinear photonic crystal

Dunzhao Wei,[1] Yunzhi Zhu,[1] Weihao Zhong,[1] Guoxin Cui,[1] Huijun Wang,[1] Ying He,[1] Yong Zhang,[1,a)] Yanqing Lu,[1] and Min Xiao[1,2,b)]
[1]*National Laboratory of Solid State Microstructures, College of Engineering and Applied Sciences, and School of Physics, Nanjing University, Nanjing 210093, China*
[2]*Department of Physics, University of Arkansas, Fayetteville, Arkansas 72701, USA*

(Received 22 March 2017; accepted 15 June 2017; published online 27 June 2017)

Based on nonlinear holography, we propose a 2D spirally poled $LiNbO_3$ nonlinear photonic crystal that generates orbital angular momentum (OAM) states of second-harmonic (SH) waves. In this crystal, the generated SH waves from positive and negative domains have a π phase difference, which is used to compose a nonlinear Fresnel zone plate for an experimental demonstration of generating SH OAM states at the designed focusing spot. In addition, the crystal can be used to detect input OAM states of fundamental beams without significantly disturbing their wave fronts. *Published by AIP Publishing*. [http://dx.doi.org/10.1063/1.4990527]

The study of optical vortices can be traced back to the 1970s, when Vaughan and Willetts observed the helical wave front of a higher-order laser mode.[1] A helical wave front is characterized by an azimuthal phase factor $\exp il\phi$, where ϕ is the polar angle and l, which may take integer values, is the so-called topological charge (TC). However, such helical wave fronts did not receive much attention until 1992 when Allen *et al*. encountered their orbital angular momentum (OAM) property.[2] Light beams with a phase term $\exp il\phi$ carry an OAM of $l\hbar$ per photon. Because the beams exhibit annular-shaped intensity patterns with no limit on l, they have been widely used in optical tweezers, optical communications, optical storage, and imaging.[3–7] These applications strongly depend on the OAM generators. The continually changing phase with polar angle requires the OAM generators to have sufficient phase modulation capacity and smooth phase modulation. Such devices and components include spiral phase plates, holographic fork-gratings, q-plates, ring-gratings, spatially varying nano-antennas, and liquid droplets.[8–14] Recently, two studies have demonstrated that multilevel lenses and binary lenses also generate high-quality optical vortices.[15,16] The work extends the OAM generators to those with insufficient phase modulation capacity for a 2π phase shift or those with less discrete phase steps. It has directed us towards generating nonlinear OAM states using the binary-phase modulation of the second-harmonic (SH) wave in opposite domains in the nonlinear photonic crystal.

With the development of quasi-phase-matching (QPM) schemes and electric poling techniques, 1D periodically poled nonlinear photonic crystals have been widely used in harmonic generation and frequency conversion.[17–19] In 1998, the proposal by Berger to use a 2D nonlinear photonic crystal provided an abundance of reciprocal vectors,[20] which have been applied in multiple-beam second-harmonic generation (SHG) and cascaded parametric up or down conversion.[21–24] In recent years, 2D nonlinear photonic crystals were utilized to generate 1D spatial light beams based on nonlinear wave-front engineering and nonlinear volume holography as the fundamental beam propagated along the x or y axis of the crystal.[25–29] The QPM scheme still works but the wave front of the SH wave is only modulated along one direction in the transverse plane. However, when one pumps the fundamental beam along the z axis of the crystal, the whole wave front of the SH wave in the transverse plane can be modulated to generate different phenomena such as the nonlinear Talbot effect, nonlinear superfocusing, and 2D nonlinear holography.[30–33] In such schemes, the high conversion efficiency of QPM is sacrificed and the phase modulation through the domain orientation has only two phase values differing by a π phase.[34] Based on the holography theory,[16,33] the nonlinear fork grating with binary phases was the first example to generate SH OAM.[35]

In this article, we propose a spirally poled $LiNbO_3$ slice to generate the SH OAM beam by using the binary-phase modulations from opposite domains. The spiral pattern can be seen as the binarization of the interference result between a spherical wave and an optical vortex. It behaves like a Fresnel zone plate with definite focusing distances and alterable working wavelengths. A well-defined SH OAM state is observed with a designed focusing distance. In comparison to the nonlinear fork grating,[35] our method does not require phase-matching in the transverse direction. Moreover, as the reflective index is uniform, we also demonstrate its application in detecting input OAM states without significantly disturbing the wave front of the fundamental beam.

The fabrication of our sample involves three steps. The first is the generation of a spiral mask. From holography, we used a computer program to generate a spiral pattern, which results from the interference between a spherical wave with radius of curvature f and a helical wave with a TC of l [Fig. 1(a)]. In the experimental demonstration, we set $f = 6.4$ mm and $l = 2$. The pattern is mathematically expressed as $\cos(-\pi r^2/\lambda f + l\varphi)$, where r, φ, and λ are the polar radius, polar angle, and wavelength of the interference wave.

a)Electronic mail: zhangyong@nju.edu.cn
b)Electronic mail: mxiao@uark.edu

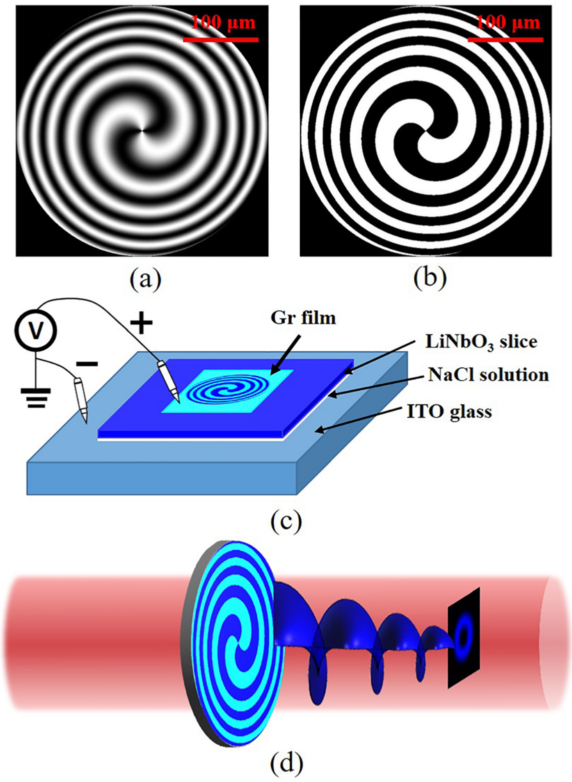

FIG. 1. (a) Interference pattern between a spherical wave with a curvature radius of $f = 6.4$ mm and a helical wave with TC of $l = 2$. (b) Binarization result of (a). (c) Poling process. A sample with a spiral pattern Cr film on the +z surface is placed on an ITO glass substrate. A thin layer of NaCl solution inserted in between them serves as a uniform electrode. A positive bias voltage is applied to the $LiNbO_3$ slice using the contacts between the sharp metal pen and Cr film. (d) Working principle for the sample. The fundamental beam passes through the sample to generate a SH OAM focused at a definite distance; the sample leaves its profile unchanged. (Scale bar, 100 μm).

However, this gradually varying pattern cannot be used in photolithography; it needs to be binarized [Fig. 1(b)]. It should be noted that the SH OAM mode produced by a binary structure is usually accompanied by high-order oscillating components. Normally, one can focus the generated SH wave to select the OAM mode because the high-order terms diverge at the focusing point. Therefore, we add a spherical wave front in the sample pattern. The second step involves transferring the binarized pattern to a 30-μm-thick z-cut $LiNbO_3$ slice by maskless photolithography. After vacuum deposition and photoresist removal, a spiral mask in a 120-nm-thickness Cr film is affixed to the +z surface of the $LiNbO_3$ slice [Fig. 1(c)]. Finally, electric poling is performed on the $LiNbO_3$ slice to ensure that the sign of the second-order nonlinear susceptibility d_{22} of the sample is tuned with $\mathrm{sgn}[\cos(-\pi r^2/\lambda f + l\varphi)]$. During poling [Fig. 1(c)], the sample is placed on an ITO glass substrate with its +z surface up. Under the –z surface, there is a thin layer of NaCl solution serving as a uniform electrode. Ten voltage pulses (pulse period, 1 s; duty cycle, 50%) with a bias voltage of 640 V, slightly larger than the coercive field (21 V/μm $\times$ 30 μm), are used to reverse the ferroelectric domain by having the positive electrode in contact with the Cr film. The changing signs of d_{22} result in a π-phase difference for the relevant SH waves when the fundamental beam propagates along the z-axis.[34] The generated SH wave front is therefore modulated by the spiral pattern [Fig. 1(d)] and is focused at the design focusing distance f. Because electric poling does not change the refractive index, the fundamental beam passes through the sample without changing its profile.

Figure 2 shows the experimental setup characterizing the SH beam property generated by the sample. A fundamental beam comes from a Ti: sapphire femtosecond-pulsed laser (pulse width, 140 fs; repetition rate, 80 MHz) operating at 900-nm wavelength. The beam is separated into a signal and reference after the beam splitter (BS). To increase the power density at the beam waist, the signal beam is focused by a lens ($f = 500$ mm) at which the sample is placed with its z-axis along the propagation direction. Both the fundamental beam and the generated SH wave from the signal arm are collected by a 10× objective lens. After the fundamental beam is filtered by a shortpass filter, only the generated SH wave at a wavelength of 450 nm is imaged by a CCD camera. The reference arm passes through a beta barium borate (BBO) crystal generating a reference SH wave. The fundamental beam is blocked by another shortpass filter. Only the reference SH wave combines with the signal SH wave in passing through another beam splitter to the CCD camera. The delay line in the reference arm is used to compensate the optical length, so that the optical length difference between the two arms is within the coherent length of the laser pulse.

We initially block the reference arm to study the propagation features of the generated SH OAM beam. The surface of the sample is placed correctly on the imaging plane of the objective with its center aligned with the center of the fundamental signal beam. We then move the imaging plane by changing the distance between the sample and the objective so that the intensity patterns of the signal SH at different propagation distances away from the surface can be recorded by the CCD camera. With a step interval of 20 μm, a sequence of SH intensity patterns within propagation distances from 5 mm to 12 mm are recorded. Figure 3(a) shows the evolution of the signal SH wave pattern; a hollow SH beam (i.e., the SH OAM mode) is clearly seen from 6 mm to 7 mm. Outside this interval, the SH beam either converges or diverges and the intensity decreases quickly. Compared with the simulation result [Fig. 3(b)], the focusing performance of the sample is nearly the same as that predicted by

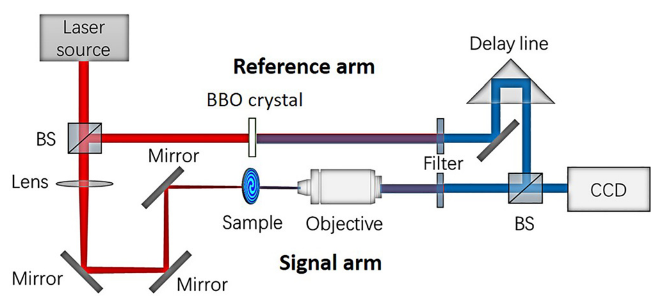

FIG. 2. The fundamental of a Ti: sapphire femtosecond-pulsed laser is separated by a beam splitter (BS) into a reference arm and a signal arm. After focusing by a lens, the signal beam is incident normally on the sample to generate a signal SH wave, which is collected by an objective and imaged on a CCD camera after the signal fundamental beam is filtered. The reference beam passes through a BBO crystal to generate a reference SH wave. After passing through a shortpass filter, it interferes with the signal SH wave following careful tuning of the delay line.

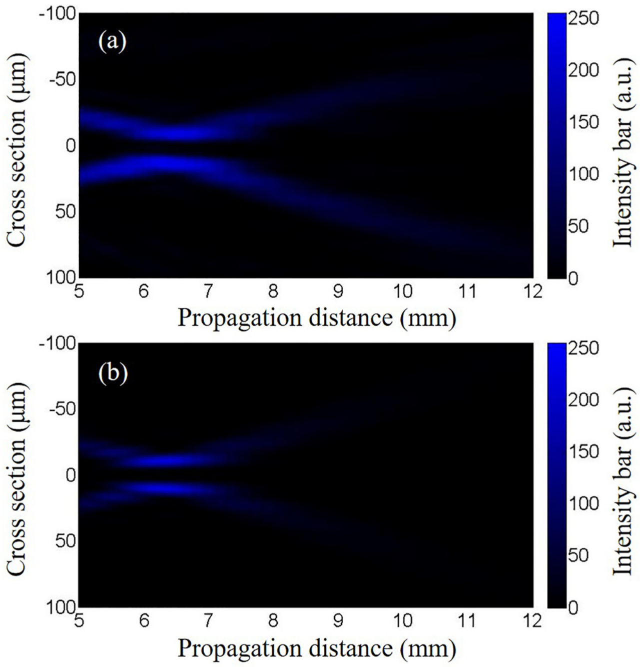

FIG. 3. (a) Experimental propagation carpet of the signal SH wave. (b) Corresponding simulation result.

the scalar diffraction theory. Because of fabrication errors, the focusing position of the sample has deviated slightly from the design focusing distance.

The SH intensity pattern at the 6.6-mm propagation distance is used to study the phase distribution and the TC of the OAM state [Fig. 4(a)]. It has a solid annular shape [Fig. 4(a)]. To reveal its helical phase front, the reference beam is unblocked allowing the reference SH wave to interfere with the signal SH wave. Because the coherent length of the laser pulse is only $\sim 20\,\mu$m, a delay line is necessary to compensate for the difference in optical length. By carefully adjusting the delay line and the beam splitter at the front of the CCD camera, the off-axis [Fig. 4(b)] and co-axis [Fig. 4(c)] interference results are imaged. The fork grating [Fig. 4(b)] directly reveals a TC with $l_S = 2$. The two petals [Fig. 4(c)] give a more apparent helical phase front distribution (*i.e.*, a 4π-phase shift along the polar angle associated with a $l_S = 2$ TC). The interference results indicate the definite TC of the OAM state.

To demonstrate the detection function of the sample, a vortex phase plate (VPP) with a TC of -1 is inserted into the signal arm. The signal beam carries a TC of $l_F = -1$ after passing through the VPP. The inset of Fig. 4(d) shows the intensity pattern of the fundamental beam transmitted through the sample. The uniform refractive index of the sample does not disturb the wavefront of the fundamental beam. However, as demonstrated before, the TC of the input beam doubles in a SHG process and the total TC of the generated SH OAM states can be expressed as $2l_F + l_S$.[35,36] In the experiment, the TC of the generated SH beam is doubled to -2 and canceled out by the TC of $l_S = 2$ carried by the sample. Therefore, one can observe a bright central spot as shown in Fig. 4(d). One finds side lobes circling the bright spot, which can be explained by the high-order oscillating terms of the Fourier expansion of the sample structure and the hollow Gaussian beam theory.[37–39] The high-order oscillating terms can be suppressed by increasing the number of zones as for the Fresnel zone plate. This can be achieved by increasing the sample size or reducing the focusing distance. For various input TCs, one has to design different spirally poled plates for their detections, which is similar to the method using a fork grating.[10] Because the phase matching condition is not satisfied under our experimental configuration, the conversion efficiency of the SH OAM mode is relatively low, which is comparable with SH OAM generation in atmospheric pressure air.[40] Therefore, such a plate has no significant influence on the fundamental wave, which provides a nondestructive way to measure the OAM information in the fundamental wave.

We have demonstrated how a holographic spirally poled nonlinear crystal of binary phase generates a SH OAM state. It integrates frequency doubling and OAM-state generation. Using holographic techniques, the focusing distance can be set at any distance, and hence, a focusing lens is not needed. A change in wavelength only affects the focusing distance, implying a large wavelength tolerance in the generation of SH OAM modes. Moreover, the thin sample leaves the wave front of the fundamental beams unchanged, which makes it a potential candidate for nondestructive OAM detection.[41] The features combine to give our sample advantages in applications such as the generation of ultraviolet OAM states for optical manipulation and super-resolution imaging or the detection of infrared OAM states in optical communications.

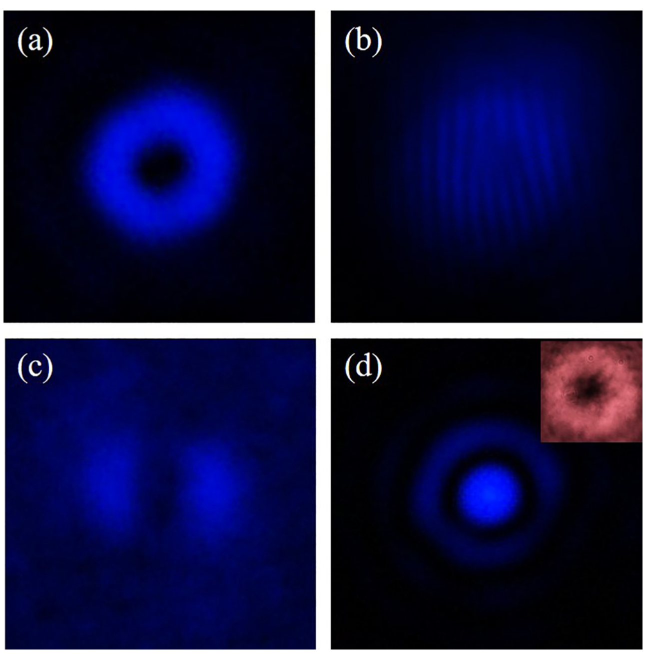

FIG. 4. (a) Signal SH intensity pattern at the propagation distance of 6.6 mm. (b) and (c) Off-axis and co-axis interference results between the signal SH wave and the reference wave at the propagation distance of 6.6 mm. (d) Counteraction result of the TCs between l_F from the fundamental beam and l_S from the sample; the inset shows the intensity pattern of the fundamental carrying a TC of -1 transmitted through the sample.

This work was supported by the National Natural Science Foundation of China (Grant Nos. 91636106, 11621091, and 61490714) and the National Basic Research Program of China (Grant Nos. 2016YFA0302500 and 2017YFA0303700).

[1]J. Vaughan and D. Willetts, Opt. Commun. **30**(3), 263–267 (1979).
[2]L. Allen, M. W. Beijersbergen, R. J. Spreeuw, and J. P. Woerdman, Phys. Rev. A **45**(11), 8185–8189 (1992).
[3]D. G. Grier, Nature **424**, 810–816 (2003).
[4]J. Wang, J. Y. Yang, I. M. Fazal, N. Ahmed, Y. Yan, H. Huang, Y. X. Ren, Y. Yue, S. Dolinar, M. Tur, and A. E. Willner, Nat. Photonics **6**, 488–496 (2012).
[5]N. Bozinovic, Y. Yue, Y. Ren, M. Tur, P. Kristensen, H. Huang, A. E. Willner, and S. Ramachandran, Science **340**, 1545–1548 (2013).
[6]A. Nicolas, L. Veissier, L. Giner, E. Giacobino, D. Maxein, and J. Laurat, Nat. Photonics **8**, 234–238 (2014).
[7]S. Furhapter, A. Jesacher, S. Bernet, and M. Ritsch-Marte, Opt. Express **13**(3), 689–694 (2005).
[8]S. S. Oemrawsingh, J. A. van Houwelingen, E. R. Eliel, J. P. Woerdman, E. J. Verstegen, J. G. Kloosterboer, and G. W. T. Hooft, Appl. Opt. **43**(3), 688–694 (2004).
[9]N. R. Heckenberg, R. McDuff, C. P. Smith, and A. G. White, Opt. Lett. **17**(3), 221–223 (1992).
[10]A. Mair, A. Vaziri, G. Weihs, and A. Zeilinger, Nature **412**, 313–316 (2001).
[11]P. Chen, B. Wei, W. Ji, S. Ge, W. Hu, F. Xu, V. Chigrinov, and Y. Lu, Photonics Res. **3**(4), 133–139 (2015).
[12]X. Cai, J. Wang, M. J. Strain, B. Johnson-Morris, J. Zhu, M. Sorel, J. L. O'Brien, M. G. Thompson, and S. Yu, Science **338**, 363–366 (2012).
[13]G. Li, M. Kang, S. Chen, S. Zhang, E. Y. Pun, K. W. Cheah, and J. Li, Nano Lett. **13**, 4148–4151 (2013).
[14]E. Brasselet, N. Murazawa, H. Misawa, and S. Juodkazis, Phys. Rev. Lett. **103**, 103903 (2009).
[15]E. Rueda, D. Muneton, J. A. Gomez, and A. Lencina, Opt. Lett. **38**(19), 3941–3944 (2013).
[16]N. Londoño, E. Rueda, J. A. Gómez, and A. Lencina, Appl. Opt. **54**(4), 796–801 (2015).
[17]J. A. Armstrong, N. Bloembergen, J. Ducuing, and P. S. Pershan, Phys. Rev. **127**(6), 1918–1939 (1962).
[18]S. Zhu, Y. Zhu, and N. Ming, Science **278**, 843–846 (1997).
[19]M. M. Fejer, G. A. Magel, D. H. Jundt, and R. L. Byer, IEEE J. Quantum Electron. **28**(11), 2631–2654 (1992).
[20]V. Berger, Phys. Rev. Lett. **81**(19), 4136–4139 (1998).
[21]Y. Zhang, Z. D. Gao, Z. Qi, S. N. Zhu, and N. B. Ming, Phys. Rev. Lett. **100**, 163904 (2008).
[22]N. G. R. Broderick, R. T. Bratfalean, T. M. Monro, D. J. Richardson, and C. M. de Sterke, J. Opt. Soc. Am. B **19**(9), 2263–2272 (2002).
[23]J. Liao, J. He, H. Liu, H. Wang, S. Zhu, Y. Zhu, and N. Ming, Appl. Phys. Lett. **82**(19), 3159–3161 (2003).
[24]S. Carrasco, M. B. Nasr, A. V. Sergienko, B. E. Saleh, M. C. Teich, J. P. Torres, and L. Torner, Opt. Lett. **31**(2), 253–255 (2006).
[25]X. H. Hong, B. Yang, C. Zhang, Y. Q. Qin, and Y. Y. Zhu, Phys. Rev. Lett. **113**(16), 163902 (2014).
[26]T. Ellenbogen, N. Voloch-Bloch, A. Ganany-Padowicz, and A. Arie, Nat. Photonics **3**, 395–398 (2009).
[27]Y. Q. Qin, C. Zhang, Y. Y. Zhu, X. P. Hu, and G. Zhao, Phys. Rev. Lett. **100**, 063902 (2008).
[28]D. Liu, D. Wei, Y. Zhang, J. Zou, X. P. Hu, S. N. Zhu, and M. Xiao, Opt. Express **21**(12), 13969–13974 (2013).
[29]S. Trajtenberg-Mills, I. Juwiler, and A. Arie, Laser Photonics Rev. **9**(6), L40–L44 (2015).
[30]Y. Zhang, J. Wen, S. N. Zhu, and M. Xiao, Phys. Rev. Lett. **104**, 183901 (2010).
[31]D. Liu, Y. Zhang, J. Wen, Z. Chen, D. Wei, X. Hu, G. Zhao, S. N. Zhu, and M. Xiao, Sci. Rep. **4**, 6134 (2014).
[32]S. M. Saltiel, D. N. Neshev, R. Fischer, W. Krolikowski, A. Arie, and Y. S. Kivshar, Jpn. J. Appl. Phys. **47**(8), 6777–6783 (2008).
[33]B. Yang, X. H. Hong, R. E. Lu, Y. Y. Yue, C. Zhang, Y. Q. Qin, and Y. Y. Zhu, Opt. Lett. **41**(13), 2927–2929 (2016).
[34]D. Wei, D. Liu, X. Hu, Y. Zhang, and M. Xiao, Laser Phys. Lett. **11**(9), 095402 (2014).
[35]N. V. Bloch, K. Shemer, A. Shapira, R. Shiloh, I. Juwiler, and A. Arie, Phys. Rev. Lett. **108**, 233902 (2012).
[36]X. Fang, G. Yang, D. Wei, D. Wei, R. Ni, W. Ji, Y. Zhang, X. Hu, W. Hu, Y. Q. Lu, S. N. Zhu, and M. Xiao, Opt. Lett. **41**(6), 1169–1172 (2016).
[37]Y. Cai, C. Lu, and Q. Lin, Opt. Lett. **28**(3), 1084–1086 (2003).
[38]C. Wei, X. Lu, G. Wu, F. Wang, and Y. Cai, Appl. Phys. B **115**, 55–60 (2014).
[39]N. Apurv Chaitanya, M. V. Jabir, J. Banerji, and G. K. Samanta, Sci. Rep. **6**, 32464 (2016).
[40]M. Beresna, P. G. Kazansky, Y. Svirko, M. Barkauskas, and R. Danielius, Appl. Phys. Lett. **95**, 121502 (2009).
[41]D. Wei, Y. Wang, D. Liu, Y. Zhu, W. Zhong, X. Fang, Y. Zhang, and M. Xiao, ACS Photonics **4**(4), 996–1002 (2017).